Z. Phys. D 37, 219–230 (1996)

ZEITSCHRIFT
FÜR PHYSIK D

The interaction of metastable helium atoms with alkaline earth atoms: He*(2^3S,2^1S)+Mg, Ca, Sr and Ba

M.-W. Ruf[1], **A.J. Yencha**[1,*], **H. Hotop**[1], **M. Movre**[2,**], **C. Kerner**[2], **S. Zillig**[2], **W. Meyer**[2]

[1] Fachbereich Physik, Universität Kaiserslautern, D-67653 Kaiserslautern, Germany
[2] Fachbereich Chemie, Universität Kaiserslautern, D-67653 Kaiserslautern, Germany

Received: 27 November 1995 / Final version: 22 January 1996

Abstract. We have carried out experimental and theoretical studies of Penning ionization processes occurring in thermal energy collisions of state-selected metastable He*(2^3S) and He*(2^1S) atoms with ground state alkaline earth atoms $X(X = \mathrm{Mg, Ca, Sr, Ba})$. Penning ionization electron energy spectra for these eight systems, measured with a crossed-beam set-up perpendicular to the collision velocity at energy resolutions 40–70 meV, are reported; relative populations of the different ionic X^+ $(m\ell)$ states are presented and well depths D_e^* for the He* + X entrance channel potentials with uncertainties around 25 meV are derived from the electron spectra as follows: He*(2^3S) + Mg/Ca/Sr/Ba: 130/250/240/260 meV; He*(2^1S) + Mg/Ca/Sr/Ba: 300/570/550/670 meV. The spectra show substantial differences for the three ionic states $X^+(^2S)$, $X^+(^2P)$ and $X^+(^2D)$ and reveal that transitions to a repulsive potential – attributed to $\mathrm{He} + X^+(^2P)\ ^2\Sigma$ formation – are mainly involved for the $X^+(^2P)$ channel. Ab initio calculations of potential curves, autoionization widths, electron energy spectra and ionization cross sections are reported for the systems He*(2^3S) + Ca and He*(2^1S) + Ca. The respective well depths D_e^* are calculated to be 243(15) meV and 544(15) meV; the ionization cross sections at the experimental mean energy of 72 meV amount to 101 Å^2 and 201 Å^2, respectively. Very good overall agreement with the experimental electron spectra is observed.

PACS: 31.50.w; 31.20.Di; 34.50.-s; 34.20.Cf; 34.20.Mq; 35.20.Gs; 52.20.Hv

1 Introduction

The group IIa and IIb elements X represent quasi-two electron systems which are characterized by substantial electron correlation effects. In direct ionization of the outer shell (dominant configuration $ms^2\ ^1S_0$) one observes appreciable populations of excited ionic states $X^+(n\ell\ ^2L)$ besides the pre-dominantly formed ground state $X^+(ms\ ^2S)$, both in photoionization [1, 2] and in Penning ionization processes involving metastable rare gas atoms Rg* [3–8]

$$\mathrm{Rg^*} + X \rightarrow \mathrm{Rg} + X^+(ms\ ^2S) + \mathrm{e}^- \quad (1a)$$

$$\rightarrow \mathrm{Rg} + X^{+*}(n\ell\ ^2L) + \mathrm{e}^-. \quad (1b)$$

The occurrence of excited ionic states X^{+*} in reaction (1b) has been detected by Penning ion optical spectroscopy PIOS [9–16] and through Penning ionization electron spectrometry PIES [3–8]. These studies were in part motivated by their connection to laser media (e.g. the He–Cd laser [17]). PIOS of excited group IIa (Mg^+, Ca^+, Sr^+, Ba^+) and group IIb (Zn^+, Cd^+) ions [9–16], most notably the work by Schearer and coworkers, has led to new insight into the Penning process through the detection of spin and coherence transfer from optically-pumped He*(2^3S) atoms [9–12, 18]. Fahey et al. [19, 20] observed significant linear polarisation of the resonance radiation $X^+(mp\ ^2P_{3/2} \rightarrow ms\ ^2S_{1/2})$ in thermal energy collisions of unpolarized He*(2^3S) atoms with $X = \mathrm{Ca, Sr, Ba}$. This polarization proves non-statistical population of the Σ and Π states in the excited $\mathrm{He} + X^+(mp\ ^2P_{3/2})$ quasi-molecule which is formed upon electron emission in process (1b). PIES of group IIb atoms was pioneered by Cermák and Herman [3, 5] and Niehaus and coworkers [4, 21] and was later studied again by Inaba et al. [7] who also included the group IIa element Mg [8]. Hotop and coworkers investigated Penning and photoionization of Ba (as well as Ce and Y) by mass spectrometry [22] and high resolution electron spectrometry [6]. They found [22] – thereby quantifying previous observations of Arrathoon et al. [23] – that double ionization is a minor channel (<2% for Ba) in Penning ionization with

Dedicated to Zdenek Herman on the occasion of his 60th birthday

* *Permanent address*: Department of Physics, State University of New York, Albany, NY, USA
** *Permanent address*: Institute of Physics, University of Zagreb, 10000 Zagreb, Croatia

metastable He* atoms and that the probability for formation of excited $Ba^+(6p)$ or $Ba^+(5d)$ ions amounts to (20–35)% of that for $Ba^+(6s)$ [6]. They discussed to some extent [6] electron exchange processes thought to be responsible for the different ionization channels (see also the work of Dalidchik [24]). In a more recent study of the similar system $He^*(2^3S) + Yb$, Hotop et al. [25] interpreted formation of excited ion states ($Yb^+(6p)$, $Yb^+(4f^{-1})$) in terms of partial autoionization width functions $\Gamma_f(R)$ which were semiempirically constructed from the electron densities for the 6*s*, 6*p*, and 4*f* orbitals as obtained in a relativistic multiconfiguration Dirac-Fock calculation for Yb. It was assumed that the Penning process (1) can be treated in the framework of local complex potential theory: autoionization proceeds from the excited entrance channel described by the complex potential $V_c(R) = V^*(R) - i\Gamma(R)/2$ to the electronic continua – built on the final ionic exit channels $V_f^+(R)$ – with partial widths $\Gamma_f(R)$ ($\Gamma(R) = \sum_f \Gamma_f(R)$). Detailed experimental and theoretical ab initio studies of the basic Penning ionization systems $He^*(2^3S) + H(1s)$ [26] and $He^*(2^1S) + H(1s)$ [27] have recently demonstrated the validity of the local complex potential theory through the very good agreement of measured and calculated angle-differential electron energy spectra for these two cases. In this connection we may note that almost 30 years ago Herman and Cermák [28] have provided one of the first insightful discussions of the mechanism for Penning and associative ionization in terms of the relevant potential curves.

Continuing our previous efforts to characterize in detail the interaction of metastable rare gas atoms with atoms X [25–27, 29–35] we now present a thorough discussion of $He^*(2^3S, 2^1S)$ Penning ionization of the alkaline earth atoms X = Mg, Ca, Sr and Ba. From high resolution electron spectra for these eight systems we deduce branching ratios for the population of the most important ionic states $X^+(^2L)$ and estimates for the well-depths D_e^* of the entrance channel potential $V^*(R)$. In accordance with expectations for the respective long-range interactions the well-depths for the $(He^*(2^1S) + X)\ ^1\Sigma$ systems are substantially deeper than those for $(He^*(2^3S) + X)\ ^3\Sigma$ (note that the triplet and the singlet potentials do not interact as a result of their different symmetry). For the systems $He^*(2^3S, 2^1S) + Ca$ as an example we present ab initio calculations of the relevant entrance and exit channel potentials $V^*(R)$ and $V_f^+(R)$ as well as partial autoionization widths $\Gamma_f(R)$ for the important ionization channels *f*. These are used to compute total and partial ionization cross sections and electron energy distributions for comparison with the experimental spectra.

In the next section we briefly describe the experimental procedure and apparatus. In Sect. 3 we present the experimental results and a comparison with available previous data. The ab initio calculations of the potential curves will be summarized in Sect. 4, followed by a discussion of the cross sections and electron energy spectra.

2 Experimental apparatus and method

The PIES apparatus used in the present work was previously described in connection with an electron spectrometric study of $He^*(2^3S, 2^1S)$ + alkali atom collisions [31]. Briefly, a well-collimated (1 : 100) metastable $He^*(2^3S, 2^1S)$ beam, originating from a differentially pumped dc cold cathode discharge source, is crossed with a collimated (1 : 30) alkaline earth target beam in a magnetically-shielded, field-free region. Electrons released in ionizing collisions between the two beams are sampled in a direction perpendicular to both beams and imaged by retarding field optics onto the entrance slit of a double hemispherical condenser, operated at a pass energy of 9.6 eV and a nominal resolution of 36 meV (FWHM). The electrons are detected with a channel multiplier and counted and stored by a multichannel scaler, the channels of which are switched synchronously with a digital voltage applied to the retarding field optics of the spectrometer. The energy scale and the effective energy resolution are determined by simultaneously measuring the well-known PI electron spectrum of Ar [36] which is admitted to the reaction region at a suitable density. The spectra were accumulated over limited time intervals and later added in order to account for surface potential variations; an overall resolution of about 70, 60, 50 and 40 meV was achieved for Mg, Ca, Sr and Ba, respectively. At the used pass energy of 9.6 eV, the transmission of the electron spectrometer was found to vary weakly between 10 and 1 eV [31]; towards higher energies the transmission was not determined for lack of suitable calibration spectra. In order to estimate uncertainties in the relative band intensities we assumed that the transmission ranged between constant and $1/\varepsilon$ behaviour (ε = electron energy).

The metastable He* beam has supersonic character with an average velocity $\bar{v}_{He} = 1750$ m/s and a velocity width $\Delta v/\bar{v}_{He}$ (FWHM) of 31% [31]. From this and the effusive beam velocity distribution of the crossed alkaline earth atoms ($T \approx 1100\ K$), relative collision energy distributions have been calculated, yielding average collision energies of $\bar{E}_{rel} = 77$, 72, 68 and 67 meV for Mg, Ca, Sr and Ba, respectively. The mixed metastable $He^*(2^3S, 2^1S)$ beam contains 6.9 times more $He^*(2^3S)$ than $He^*(2^1S)$ atoms with an estimated uncertainty of this flux ratio of $\leq \pm 25\%$, see appendix of [31]. It could be state-selected by irradiation from a cooled helical He discharge, surrounding the He* beam for about 50 mm, resulting in effective (>99%) and selective removal of $He^*(2^1S)$ atoms [31]. For the lighter alkaline earth atoms Mg, Ca and Sr, this quenching method was applied for short test runs only, and it was verified that the respective $He^*(2^1S)$ and $He^*(2^3S)$ PI electron spectra exhibit nearly no overlap. Only for Ba, the $He^*(2^1S)$ component of the metastable helium beam had to be removed in order to obtain a pure $He^*(2^3S)$ electron spectrum and to extract the $He^*(2^1S)$ electron spectrum by appropriate subtraction.

3 Experimental results and qualitative discussion

In Fig. 1 the measured energy spectra of electrons due to the reactions

$$He^*(2^1S, 2^3S) + X(^1S) \rightarrow He + X^+(^2S, ^2P, ^2D) + e^-$$

(X = Mg, Ca, Sr, Ba) are plotted on a common energy scale, i.e. relative to the respective nominal energies

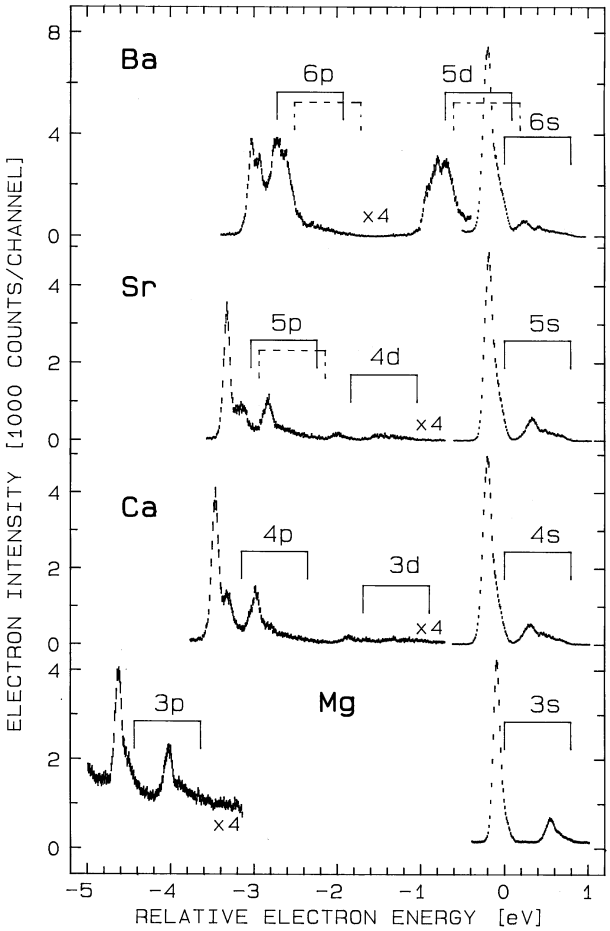

Fig. 1. Electron energy spectra resulting from ionizing collisions of metastable He*(2^3S, 2^1S) atoms with alkaline earth atoms X = Mg, Ca, Sr, Ba at average collision energies around 70 meV (see text). The spectra are plotted on a common energy scale relative to ${}^3E_0(X^+(ms))$ for formation of ground state ions. The *twin bars* indicate the positions of the nominal energies ${}^3E_0(X^+(m\ell))$ for He*(2^3S) + $X \rightarrow$ He + $X^+(m\ell)$ + e$^-$ (*left*) and ${}^1E_0(X^+(m\ell))$ for He*(2^1S) + $X \rightarrow$ He + $X^+(m\ell)$ + e$^-$ (*right*). For $X^+(ms\,{}^2S_{1/2})$, $X^+(mp\,{}^2P_{3/2})$, and $X^+((m-1)d\,{}^2D_{5/2})$ *full bars* have been used; in the cases of Sr and Ba, the $X^+(mp^2P_{1/2})$ and $X^+((m-1)d\,{}^2D_{3/2})$ states are indicated in addition by *broken lines*

${}^3E_0(X^+({}^2S))$ defined as excitation energy of He*(2^3S) minus ionization energy of X for the ionic ground state. The (relative) nominal energy positions of the ionic ground and excited states are indicated by pairs of vertical lines, the left one referring to He*(2^3S) PI and the right one to He*(2^1S) PI. In all cases the peaks of the electron spectra are considerably shifted towards lower electron energies with respect to the nominal energy positions, indicating substantial attraction in the entrance channel (see below).

The measured energy shifts are listed in Table 1 as $E_0 - \varepsilon_m$ where E_0 is the nominal energy and $\varepsilon_m \equiv \varepsilon(R_m)$ corresponds to the respective minimum of the difference potential between the entrance and exit channels [37, 38]:

$$\varepsilon(R) = V^*(R) - V^+(R). \tag{2}$$

Classically, the ionization probability per unit energy range $P(\varepsilon)$ is connected with the ionization probability per unit distance range $\hat{P}(R)$ by

$$P(\varepsilon) = \hat{P}(R)/|\mathrm{d}\varepsilon/\mathrm{d}R| \equiv \hat{P}(R)/|\varepsilon'(R)|. \tag{3}$$

For a minimum $\varepsilon(R_m)$ in the difference potential at some distance R_m, formula (3) yields an integrable singularity in $P(\varepsilon)$ [37]; in a semiclassical treatment [38], based on a harmonic difference potential $\varepsilon(R)$ and a constant width function, the term $1/|\varepsilon'(R)|$ is replaced by the square of an Airy function for which ε_m corresponds to the special low energy point where $P(\varepsilon)$ has dropped to 43.8% of its peak value. Depending on the true shape of the width function and on the collision energy this relation between ε_m and the low energy edge of the spectrum may change somewhat (see e.g., [30]). In the purely theoretical electron spectra obtained in this work for He*(2^3S, 2^1S) + Ca (as computed for the experimental distribution of collision energies, but not convoluted with the resolution function of the electron spectrometer, see Fig. 6) the minima of the difference potentials correspond to 35% to 55% fractions of the peak intensity for the different cases. However, the 43.8% energy points in the theoretical spectra differ from the respective ε_m values by at most 11 meV. In view of these small differences and missing theoretical data for He* + Mg, Sr, Ba we have chosen to consistently determine the ε_m values presented in Table 1 on the basis of the 43.8% criterion as applied to resolution-corrected spectra. The listed error limits include the uncertainties connected with the possible deviation of the true ε_m position from the 43.8% value. The resolution correction was carried out on the basis of the effects which the convolution by the appropriate spectrometer function had on the respective low energy edges Airy-type model spectra.

The well depth D_e^* for the entrance channel $V^*(R)$ is determined from the $\varepsilon_{m,s}$ values for the ground exit channel He + $X^+(ms)$. The corresponding ionic potential $V_s^+(R)$ varies only slowly at distances around R_m; therefore, the equilibrium distance R_e^* of the entrance channel potential is nearly equal to R_m, and one obtains the following simple equation for the well depth [31]

Table 1. Shifts of the minima ε_m in the respective difference potentials relative to the nominal energies E_0 (excitation energy of He*($2^{1,3}S$) minus ionization potential of X) and well depths D_e^* for the He*(2^3S) + X and He*(2^1S) + X systems (see text for evaluation procedure)

	X =	Mg	Ca	Sr	Ba
He*(2^3S) + X					
$E_0 - \varepsilon_m$[meV]	$X^+({}^2S)$	130(20)	250(20)	240(20)	260(20)
	$X^+({}^2P_{3/2})$	220(20)	350(20)	330(20)	350(20)
	$X^+({}^2D_{5/2})$	–	240(40)	220(30)	250(40)
D_e^*[meV]		130(25)	250(25)	240(25)	260(25)
He*(2^1S) + X					
$E_0 - \varepsilon_m$[meV]	$X^+({}^2S)$	300(20)	570(20)	550(20)	670(30)
	$X^+({}^2P_{3/2})$	440(20)	690(30)	660(30)	730(60)
	$X^+({}^2D_{5/2})$	–	500(40)	540(30)	610(60)
D_e^*[meV]		300(25)	570(25)	550(25)	670(35)
$\frac{D_e^*(2^1S)}{D_e^*(2^3S)}$		2.31	2.28	2.29	2.58

Table 2. Branching ratios into the X^+ final ionic states and total cross section ratio for He*(2^1S)/He*(2^3S) Penning ionization of the alkaline earth atoms X

	$X =$	Mg[a]	Mg[b]	Ca[a]	Sr[a]	Ba[a]	Ba[c]
Branching ratios							
He*(2^3S) + X	$X^+(^2S)$	100	100	100	100	100	100
	$X^+(^2P)$	15(4)	15	17(3)	15(2)	30(4)	35(6)
	$X^+(^2D)$	–	–	1.0(3)	0.9(2)	22(1)	20(4)
He*(2^1S) + X	$X^+(^2S)$	100	100	100	100	100	100
	$X^+(^2P)$	49(16)	24	45(7)	34(5)	34(6)	25(10)
	$X^+(^2D)$	–	–	5.0(7)	6.6(8)	24(3)	25(10)
Cross section ratio							
He*(2^1S)/He*(2^3S)		1.8(9)[d]	2.4	1.8(5)[d]	1.8(5)[d]	1.3(3)[d]	

[a] Present work (listed uncertainties reflect statistical errors and the limited knowledge of the spectrometer transmission, see Sect. 2)
[b] [8] data obtained with a retarding field analyzer of about 0.35 eV resolution and a mixed metastable He* beam
[c] [6] data obtained with a 127° cylindrical analyzer of 30–50 meV resolution and with a mixed He*(2^1S, 2^3S) or a pure He*(2^3S) beam. The spectrometer transmission was assumed to be constant in the energy range of interest
[d] Error estimate includes a ±25% uncertainty of the $2^3S/2^1S$ flux ratio (see Sect. 2 and [31])

(we set $V_s^+(\infty) = 0$)

$$D_e^* \approx E_0 - \varepsilon_{m,s} - V_s^+(R_e^*). \quad (4)$$

For the ionic ground states $X^+(ms, {}^2S_{1/2})$, the He*(2^1S) induced PI electron spectra are broader (widths 0.5–0.8 eV) than the He*(2^3S) spectra (widths 0.4–0.5 eV); they exhibit clear structure, and their shifts of the low energy edge are larger by 170–410 meV (see Table 1), indicating stronger entrance channel interactions for He*(2^1S) + X than for He*(2^3S) + X. The opposite situation was met for He*(2^1S) and He*(2^3S) PI of the alkali atoms Li to Cs [31]. Also in contrast to these alkali PI systems, the present alkaline earth PI systems exhibit considerable excited state formation, especially in the $X^+(mp)$ channel (see Fig. 1 and Table 2). The $X^+((m-1)d)$ states are also clearly observed; for Ba^+ they attain a similar strength as the resonance states $X^+(mp)$ as reported and discussed previously [6]. For He*(2^3S) + Mg, Sr we also detected the $X^+((m+1)s)$ excited state with a relative intensity of 0.3(2)% and 0.7(4)% relative to the $X^+(ms)$ ground state. Previous intensities for He*(2^3S) + Mg [8] are in satisfactory agreement with our findings.

For the excited ionic states $X^+(mp)$ (less clearly for $Mg^+(3p)$) the He*(2^3S) induced PI electron spectra consist of two components which we attribute to the Π–Σ-splitting of the corresponding ionic exit channel potential energy curves (see below). The low energy edge shifts of the main components can be easily determined and are all about 100 meV larger than those for the respective ionic ground states (see Table 1), indicating repulsive interaction in the excited ionic exit channels. With respect to energy shifts, the same situation is met for the He*(2^1S) induced PI electron spectra for $X^+(mp, {}^2P_{3/2})$ formation. But in this case the Π–Σ-splitting is obscured by the broad structure already present in the respective ionic ground state spectrum which, obviously, is due to the strong He*(2^1S) + X entrance channel interaction. For $X^+((m-1)d, {}^2D_{5/2})$ formation (X = Ca, Sr, Ba), the energy shifts are more or less the same as for the respective ionic ground states, for both He*(2^1S) and He*(2^3S) PI. The estimated uncertainties are quite large either due to poor statistics (Ca, Sr) or due to the strange shape of the $Ba^+({}^2D_{5/2})$ low energy edge (see Figs. 1 and 2). Therefore, we can only conclude that in the relevant internuclear distance range the final state interactions for $X^+((m-1)d, {}^2D)$ formation are about the same as for $X^+(ms, {}^2S)$.

Figure 2 shows the measured PI electron spectra of barium plotted on an absolute electron energy scale, the above mentioned overlap of He*(2^1S) and He*(2^3S) induced PI electron spectra is clearly seen by comparing the mixed metastable PI electron spectrum (lower trace) and the pure He*(2^3S) induced one (middle trace) where the He*(2^1S) metastable beam component had been effectively quenched. The pure He*(2^1S) induced PI electron spectrum (upper trace) was generated by subtraction of the two former spectra after proper normalization. The barium ionic ground state (6s) PI electron spectra exhibit very similar shapes when compared with the other alkaline earth PI systems (Mg, Ca, Sr), for both He*(2^1S) and He*(2^3S) PI. For He*(2^3S) PI, the barium ionic excited states (6p and 5d) electron spectra are characterized by complicated structures (see Fig. 2, middle trace) which we attribute to enhanced contributions of the second fine structure components ${}^2P_{1/2}$ and ${}^2D_{3/2}$, respectively, and to complex shapes of the exit channel potentials leading to ${}^2P_{3/2}$ and ${}^2D_{5/2}$ formation. For He*(2^1S) PI, the barium ionic excited states electron spectra suffer from rather poor statistics (see Fig. 2, upper trace) and large error bars have therefore been attributed to the shifts of the low energy edges for Ba^+ ${}^2P_{3/2}$ and ${}^2D_{5/2}$ (see Table 1) and to the respective final state branching ratios (see Table 2). The latter are in satisfactory agreement with previous experimental data [6]. On the other hand, Gérard et al. [6] reported for the entrance channel potentials of He*(2^3S) + Ba and He*(2^1S) + Ba well depths of 0.37(4) eV and 0.81(8) eV, respectively. We note that their published electron spectrum for He*(2^3S) + Ba is in good agreement with the present data; in particular the values

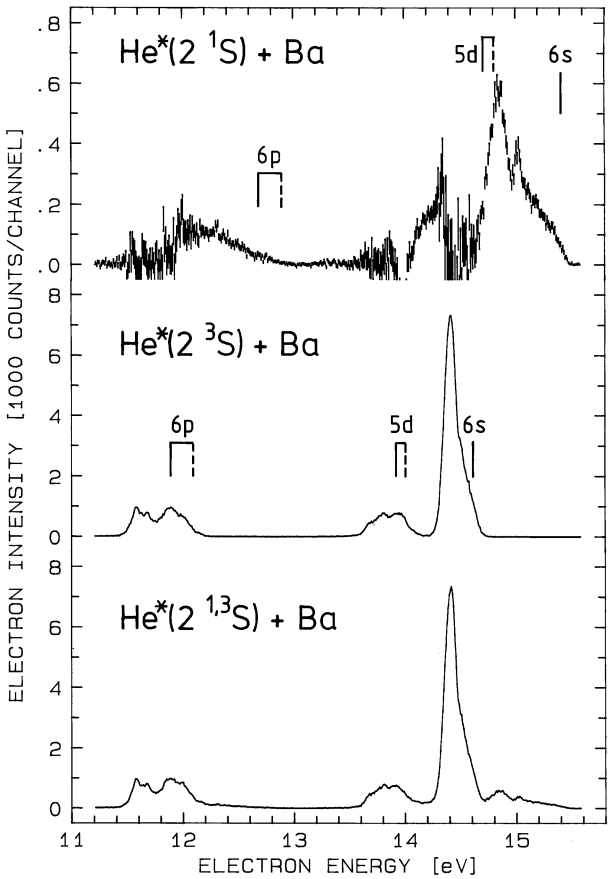

Fig. 2. Electron energy spectra resulting from ionizing collisions of metastable He*(2^3S, 2^1S) atoms with Ba atoms (average collision energy 67 meV). The He*(2^1S) + Ba spectrum was generated by subtraction of a pure He*(2^3S) + Ba spectrum from the mixed He*(2^3S, 2^1S) + Ba spectrum. The *vertical lines* indicate the respective nominal energies (see Fig. 1)

ε_m for the low energy edges in the respective $Ba^+(6s)$ peaks agree to within 20 meV. Re-evaluation of their Penning electron spectra for the systems He*(2^3S), He*(2^1S), Ne*($3s$, $^3P_2$) + Ba shows that the well depths quoted in [6] are incorrect and generally too high by about 100 meV.

Since no other information about the entrance channel potentials of the studied He* + X systems has been available prior to this work we make use of the well-known chemical similarity between He*(2^3S) and Li($2s$) [31]. The molecular bonding in LiMg and LiCa was treated theoretically by Jones [39] and the binding energies were calculated as 170 meV and 270 meV, respectively, showing qualitative agreement with our results for $E_0 - \varepsilon_m$ of $2^3S/Mg^+(3s)$, $Ca^+(4s)$ (see Table 1). For a more precise evaluation one has to consider the exit channel attraction (see eq. (4)), i.e. the equilibrium distance R_e^* of the entrance channel potential $V^*(R)$ has to be estimated and reasonable assumptions about the exit channel potential $V^+(R)$ have to be made. Following the lines of [31], we start from the theoretical equilibrium distances calculated by Jones [39] as 6.04 a_0 and 6.66 a_0 for LiMg and LiCa, respectively, and add about 0.5 a_0 for He*(2^3S) + Mg and He*(2^3S) + Ca, arriving at about 6.5 a_0 and 7.2 a_0. At very large internuclear distances the exit channel

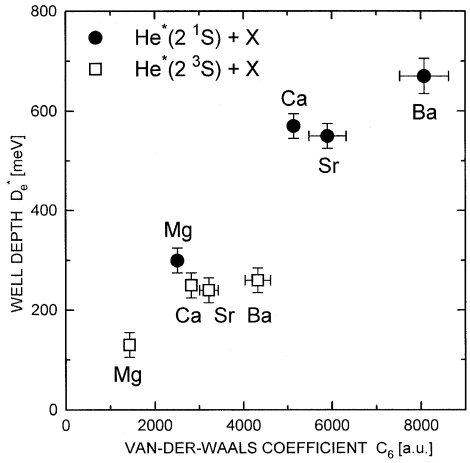

Fig. 3. Correlation between the experimentally determined well depths D_e^* for the He*(2^3S) + X and He*(2^1S) + X systems (X = Mg, Ca, Sr, Ba) and the respective Slater-Kirkwood C_6 coefficients (see Table 3) for the long range C_6/R^6 van der Waals attraction

Table 3. Polarizabilities α and van der Waals coefficients C_6 (Slater-Kirkwood formula) for He* + X systems

X	$\alpha_X[a_0^3]$	He*(2^3S) + X C_6[a.u.][a]	He*(2^1S) + X C_6[a.u.][a]	$\frac{C_6(2^1S)}{C_6(2^3S)}$
Mg	72(2)[b]	1426(28)	2506(50)	1.76(5)
Ca	159[c]	2821(24)	5133(46)	1.82(3)
		2398[c]	3818[c]	1.59[c]
Sr	186(15)[b]	3217(209)	5898(418)	1.83(18)
Ba	268(22)[b]	4323(288)	8073(549)	1.87(18)

[a] Calculated with (5) (see text) using α(He*(2^3S)) = 315.63 a_0^3 [40] and α(He*(2^1S)) = 801.10 a_0^3 [40]
[b] Recommended values of [40]
[c] Theoretical values from the present work; estimated uncertainty: 1% for α, 2% for C_6

He + X^+(X = Mg, Ca) is dominated by charge-induced dipole interaction due to the polarizability of helium (α_{He} = 1.38 a_0^3 [40]), but this is not true at the relevant distances of about 6.5 a_0 due to the large size of the X^+ valence orbital. The ab initio potential for He + $Ca^+(4s)$ $^2\Sigma$ (see Sect. 4) exhibits a weak well near 8 a_0 and goes through zero ($V_s^+(\infty) = 0$) near R = 7 a_0. Therefore we use the estimate $V_s^+(R_e^*) = (0 \pm 5)$ meV in eq. (4) for deriving well depths D_e^* from the measured values $E_0 - \varepsilon_{m,s}$, as summarized in Table 1.

Since the ground states of the alkaline earth atoms form closed shells (even though highly correlated), the entrance channel attraction is largely of dispersion origin and should correlate well with the long range coefficient C_6. This (qualitative) correlation is visualized in Fig. 3 in which we have plotted the experimentally determined well depths D_e^* versus the C_6 coefficients for He* + X as obtained from the Slater-Kirkwood formula [40]

$$C_6(X + \text{He}^*) = (3/2)\alpha_X \cdot \alpha_{\text{He}^*}[(\alpha_X/2)^{1/2} + (\alpha_{\text{He}^*})^{1/2}]^{-1} \text{ [a.u.]} \quad (5)$$

using the polarizabilities α given in Table 3. The connection between D_e^* and C_6 is especially clearly borne out

when one compares the ratios of the C_6 coefficients with the ratios of the well depths D_e^* for $He^*(2^1S) + X$ and $He^*(2^3S) + X$, respectively: as listed in Tables 1 and 3 both ratios are nearly constant.

We note that the trends just discussed for $He^* + X$ are reversed for the respective alkali (A) target systems, where the entrance channel attractions were found to decrease from the lighter ($A = Li$) to the heavier ($A = Cs$) target atoms and to differ by factors of 2 to 3 between $He^*(2^1S)$ and $He^*(2^3S)$ PI in favour of the latter [31]. This behaviour is mainly due to substantial electron pair-type chemical bonding for the $(He^*(2^3S) + A)^2\Sigma^+$ potentials.

4 Ab initio calculations for the $He^*(2^3S, 2^1S) + Ca$ systems

For Penning systems like $He^*(2^3S, 2^1S) + H/D(1s^2S)$, $Li(2s^2S)$, $Na(3s^2S)$ we have recently demonstrated that the observed high-resolution electron spectra could be very well reproduced from ab initio calculated electronic structure data on the potential curves V^* and V^+ and the pertinent resonance-to-continuum coupling matrix elements by a treatment of the nuclear motion in the local complex potential approximation [26, 27, 32]. All details of a rich interference structure, including the delicate angular dependence of the spectra, appeared to be accounted for as long as no further approximation was made in the calculation of the coupling matrix elements, i.e. when the phase information in the individual coupling matrix elements $V_{f\ell}(R, \varepsilon)$ to continuum electrons of energy ε and asymptotic CM angular momentum ℓ was fully used. The theoretical procedures used in this treatment have been presented and thoroughly discussed in the context of the benchmark system $He^*(2^3S) + H(1^2S)$ [41]. It has also been shown that spectra taken perpendicular to the plane of the crossed beams are particularly close to angle-integrated spectra as obtained from an approximate theoretical treatment, introduced by Hickman and Morgner [42], in which only the total width function $\Gamma(R)$ has to be known in addition to the interaction potentials. This approximation rests on assumptions which are rather well obeyed in systems with repulsive entrance channel potentials. Typically their spectra show relatively little structure and are dominated by a single Airy peak per exit channel. Due to the closed-shell structure of the alkaline earth ground states, our collision systems are repulsive in this sense irrespective of their sizeable dispersion attraction. We therefore decided to base our treatment on this approximation thus avoiding the evaluation of the $V_{f\ell}(R, \varepsilon)$. Instead we use the rather simple Stieltjes imaging procedure to derive the pertinent width functions and place emphasis on accurate potentials. The interaction potentials indeed pose the main problem not only due to the notorious difficulties in accounting fully for dispersion type attraction but also because the marginal but positive electron affinity of Ca enhances the van der Waals attraction considerably. Its calculation is in itself rather difficult: The technical problem with weakly bound negative ions of closed shell neutral systems arises from the fact that the excess electron stays unbound – i.e. occupies a very diffuse orbital – at any level that does not account for nearly all correlation so that the final step in a CI treatment involves a drastic electron redistribution.

In order to facilitate an exhaustive treatment of the valence shell electron correlation we account for the core-valence intershell correlation by an effective core polarization potential which is based on the assumption that intershell correlation is basically due to the polarizability of the inner-shell core. The finite size of the core and corresponding penetration and exclusion effects are taken into account by a cut-off function which removes the unphysical singularity at $r \to 0$. In its simplest form this cut-off function is the same for all valence electrons and involves a single parameter which may be defined semi-empirically by adjusting the calculated ionization energy of the atom or ion to its experimental value [43]. This proved fully adequate for alkali atoms and allowed the calculation of dissociation energies and excitation energies of alkali dimers to within 50 cm^{-1} [44]. It works very well for Be and Mg also, but Ca with its low-lying and strongly core-penetrating d-orbitals requires ℓ-dependent cut-off functions, resulting in a semi-local potential.

The performance of the effective core polarization potential as well as the adequacy of the basis set used can be judged from looking at energetic properties of Ca^+, Ca, and Ca^- which are relevant for the process under consideration here. Table 4 provides a comparison of experimental data with those obtained from present core-SCF/valence-CI calculations including the core polarization potential. The excitation energies are reproduced with relative errors smaller than 0.7% with a single exception for Ca^+(3d) where it amounts to 1.5%. The calculated electron affinity matches the recent experimental values [45, 46] within the experimental error; for a comparison with previous theoretical results, see [47]. The calculated

Table 4. Atomic energies for Ca (in eV)

			Calculated[a]	Experimental[a]
Ca^-	$4s^2 4p$	^2P	−0.0187 −0.0177[b]	−0.0184(25)[c] −0.0175 + 0.0020[d] − 0.0040
Ca	$4s4s$	^1S	0.0	0.0
	$4s4p$	^3P	1.901	1.892
	$4s3d$	^3D	2.507	2.524
	$4s3d$	^1D	2.699	2.709
	$4s4p$	^1P	2.916	2.932
	$4s5s$	^3S	3.918	3.910
	$4s5s$	^1S	4.131	4.131
Ca^+	$4s$	^2S	6.115	6.113
	$3d$	^2D	7.963	7.810
	$4p$	^2P	9.261	9.255
	$5s$	^2S	12.591	12.581
Ca^{++}			17.986	17.984

[a] Relative to Ca ground state; energies correspond to multiplet centers except for experimental values for Ca^-
[b] [47]
[c] [45]
[d] [46]
The experimental energies for Ca, Ca^+ and Ca^{++} were taken from the tables of C.E. Moore [52]

dipole polarizability quoted in Table 3 is probably more reliable than the experimental value. Table 4 demonstrates that our calculations of the Penning systems are based on accurate descriptions of the atoms including their dispersion forces – He is not discussed here because its proper treatment is rather trivial and corresponding atomic data may be found in [34]. We may finally note that the GTO basis set used comprises a total of 18*s*, 14*p*, 6*d*, 3*f* and 13*s*, 5*p*, 2*d* functions for Ca and He, respectively. (The GTO basis used in the atomic Ca calculations was augmented by two *g*-functions.)

For low collision energies and relatively large energies of the ejected electrons as pertaining here, the ionization process can be treated safely within the Born-Oppenheimer appoximation. As to the electronic part of the wave function it is to be noted that the autoionizing states are not eigenstates of the electronic Hamiltonian H_{el} but represent "bound" resonance states embedded in the continua of molecular ion plus ejected electron. Thus, the coupling is provided by the electronic Hamiltonian itself. The formal definition of resonance states is usually based on a Feshbach projection [48]. Two orthogonal projection operators P and $Q = 1 - P$ are defined, and they partition the Hilbert space into one part containing the background continuum states and the other part containing the embedded resonance states. The resonance state wavefunctions Φ_* and continuum state wavefunctions $\Phi_{+f\ell}$ (describing the molecular ion in its state f and an ejected electron with angular momentum ℓ) are obtained as eigenfunctions of their respective diagonal blocks of H_{el}.

If the energetically allowed part of the electronic continuum is sufficiently complete and unstructured, the ionization can be viewed as a (vertical) Franck-Condon transition, i.e. the total electronic energy is conserved during autoionization and the electron energy ε equals the difference of the potentials $V^* - V_f^+$ at the internuclear separations where the ionization takes place. The entrance channel nuclear motion is then governed by a local complex potential the imaginary part of which accounts for the loss of entrance channel population by ionization. The local autoionization width is given by the golden-rule-like formula

$$\Gamma(R) = 2\pi \sum_{f,\ell} |V_{f\ell}(R)|^2 \tag{6}$$

where the coupling matrix elements

$$V_{f\ell}(R) = \langle \Phi_*(R)|H_{el}|\Phi_{+f\ell}(R, \varepsilon(R))\rangle \tag{7}$$

are functions of the internuclear separation R. The partial width Γ_f for a particular exit channel f can be obtained by a Stieltjes imaging procedure [49, 50, 41] from discretized L^2 representations of the continuum states $\Phi_{+f\ell}$. This constitutes the basis for the treatment of Penning ionization in the local complex potential approximation which we will adopt here.

We have implemented the Feshbach projection in ab initio multi-reference CI methods as already discussed in [26, 27, 34, 41]. The resonance states under investigation here are typical Feshbach resonances characterized by core excitation and relatively weak coupling. In such cases the Feshbach projection provides an adequate practical means to construct the resonance states. We have based the projection on the occupation pattern of the He-1*s* shell. The P space is spanned by the set of configurations which are antisymmetrized products of (open-shell) Hartree-Fock determinants for the exit channel ionic states $HeCa^+$ (with He 1*s* doubly occupied) with each of the unoccupied orbitals representing a continuum electron wave packet. The Q space is then simply the complement $Q = 1 - P$. The resonance state is calculated variationally within the Q-space by a singles–doubles multi-reference CI using the self-consistent pairs techniques [51]. All configurations are constructed from a single set of orbitals obtained as follows: The active orbitals – those asymptotically describing He 1*s*, 2*s* and Ca 4*s*, 4*p* orbitals, respectively – are adapted to the resonance state in an MC-SCF calculation (note that an accurate description of the ionic state(s) is not required to define the projection Q which may rather be chosen to be optimal for the construction of the resonance states [41]). The virtual orbitals used in the CI with Feshbach projection have been required to diagonalize the Fock operators pertaining to the $He(1s^2)Ca^+(4s)$ or $He(1s^2)Ca^+(4p)$ ions, respectively, and thus provide a discretized but uncoupled representation of the respective exit channel continua with corresponding electron energies and coupling matrix elements.

The multi-configuration reference wavefunctions are obtained from small MC-SCF calculations. Since complete active spaces are used, the calculations include the ground state as well as those P-space configurations which may be constructed from the active orbitals, but the corresponding roots are not weighted in the selfconsistency procedure. The presence of these configurations is important as they have considerable interaction with the resonance states. Using this procedure with the above described basis set leads to potentials to which we attribute an accuracy of 10 to 15 meV.

The width functions have been obtained by a variant of the Stieltjes imaging procedure as described earlier [34, 41]: for each internuclear separation R, the cumulative step function

$$I_f(\varepsilon) = 2\pi \sum_i \theta(\varepsilon - \varepsilon_i)|\langle \Phi_*|H_{el}|\Phi_{+fi}(\varepsilon_i)\rangle|^2 \tag{8}$$

has been transformed into a function of $x = \exp[-a(\varepsilon - \varepsilon(R))]$ which has then been fitted by a low-degree polynomial [34, 41]. Finally, the width functions have been derived from

$$\Gamma_f(R) = \left(\frac{\partial}{\partial \varepsilon} I_f(\varepsilon)\right)_{\varepsilon = \varepsilon(R)} . \tag{9}$$

The calculated potential curves $V^*(R)$ and $V_f^+(R)$ are displayed in Fig. 4. The characteristic data for the entrance channel potentials and the corresponding difference potentials are collected in Table 5. Good agreement is found between the calculated and experimentally determined depths of difference potentials. As already discussed the depths of the resonance potentials are clearly related to the strength of the dispersion attraction as measured by C_6. Note also that the repulsive branches of resonance and ionic states are only slightly shifted with

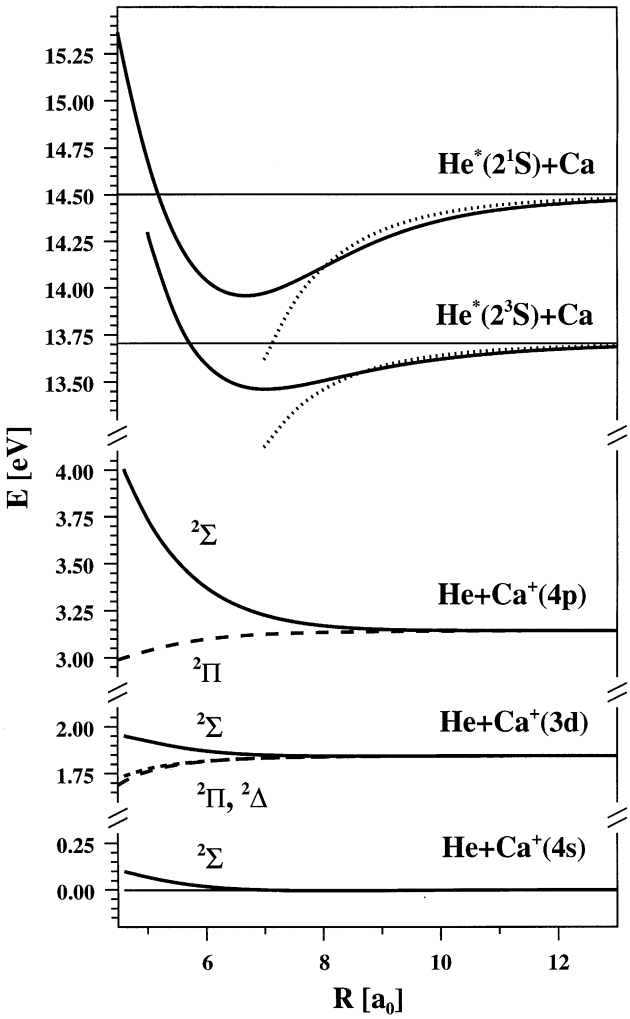

Fig. 4. Ab initio potential curves for the excited entrance and the important ionic exit channels relevant for Penning ionization in collisions of metastable He*(2^3S, 2^1S) atoms with Ca atoms (numerical values available upon request). *Dotted curves* for the resonance potentials represent the $-C_6R^{-6}$ van der Waals attraction

Table 5. Characteristic data for the resonance potentials of He*(2^1S, 2^3S) + Ca

States	He*(2^1S)	He*(2^3S)
$R_e^*(a_0)$	6.68	7.05
D_e^*(meV)	544	243
$E_0 - \varepsilon_m(4s)$(meV)	547	244
	570(20)[a]	250(20)[a]
$E_0 - \varepsilon_m(4p\Sigma)$(meV)	698[b]	361[b]
	699(30)[a,b]	359(20)[a,b]
$E_0 - \varepsilon_m(4p\Pi)$(meV)	517[b]	224[b]
C_6(a.u.)	3818	2398
C_8(a.u.)[c]	397371	317374
p_1[c]	1.19922	0.34318
p_2[c]	3.85183	5.46356
p_3[c]	1.64838	2.09742
p_4[c]	1.03924	0.83244
rms error (10^{-3}a.u.)	0.296	0.016

[a] Present experimental value (Table 1)
[b] E_0 corresponds to atomic multiplet center
[c] Fit parameters for analytical representation: $p_1 R^{p_2}\exp(-p_3 R) - C_6R^{-6}\Gamma_6(p_4R) - C_8R^{-8}\Gamma_8(p_4R)$, where Γ_n is the incomplete error function

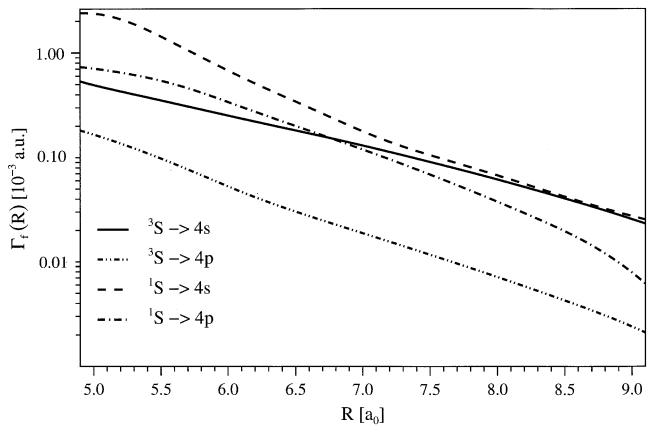

Fig. 5. Partial autoionization width functions $\Gamma_f(R)$ for Penning ionization in He*(2^3S, 2^1S) + Ca collisions leading to $Ca^+(4s)$ or $Ca^+(4p)$ ions

respect to each other, indicating a weak repulsion from the He 2*s* electron and an appreciable overlap between He 1*s* and Ca 4*s* at the turning points of thermal collisions in the resonance states. The relevant width functions corresponding to the uncoupled exit channel states are shown in Fig. 5. They show the usual overall exponential shape; they reach saturation only below 5 Bohr (not shown). The ratio between the partial widths for the 4*p* and 4*s* exit channel is remarkable, ranging from 10 to 20% for triplet He and 15 to 50% for singlet He. They explain the observed significant population of the 4*p* exit channels. It should be noted that the latter is much larger than the fractional population of $4p\sigma^2$ in the Ca ground state which amounts to 1.8% only. The large contribution from the 4*p* channel is rather to be understood as a result of the substantial admixture of a Ca 4*p* component to the original 2*s* orbital of He* (and an accompanying polarization of the 4*s* towards the He^+ center) at distances of significant ionization probability. E.g. in the triplet case with He 1*sα* occupied, the ionization involves a transition of the Ca 4*sβ* to He 1*sβ* while either the original 2*sα* is ejected (with propensity) or the 4*sα*. In this latter case the remaining electron changes dominantly to Ca^+4p after ejection. The significant occupation of the 4*p* orbital in the resonance state is related to the positive electron affinity of Ca. Indeed, the dipole moment of this state has He^+Ca^- polarity at all distances and reaches a maximum of 1.23 au at about 6 Bohr separation, consistent with an 4*p* occupation of at least 20%. Consistent with the larger 4*p*/4*s* width ratio for singlet He, the charge transfer is also larger in this case: the dipole moment reaches a maximum of 2.07 au at 6 Bohr separation. The difficulty in obtaining the proper distribution of the loosely bound electron is highlighted by the following sequence of dipole moments obtained at the SCF (−0.28), MC-SCF (−1.35) and MR-CI levels (+0.98 and +1.23 after a natural orbital iteration) in the triplet case.

The width functions pertaining to the uncoupled $4p\Pi$ exit channel turned out to be about three orders of magnitude smaller than the $4p\Sigma$ and are negligible. However, as

discussed in the previous section, the experimental spectra show small contributions from ionization to the $4p\Pi$ exit channel. We conclude that the $4p\Pi + e^-(\pi)$ exit channel "borrows" intensity from the $4p\Sigma + e^-(\sigma)$ channel due to mixing caused by the interaction between these two final states. In other words, we have to consider coupled continua within the P subspace. Couplings are provided by the electrostatic interaction involving the ejected electron as well as by the spin-orbit interaction within the molecular ion. Unfortunately, it appears difficult to assess the effective branching between the $e^-(\sigma)$ and $e^-(\pi)$ from the L^2 description of the continua. We have therefore simply chosen to adopt an empirical constant ratio between the widths $\Gamma_{p\Pi}(R)$ and $\Gamma_{p\Sigma}(R)$, as suggested by the observed spectra (see below).

5 Comparison of experimental and theoretical electron spectra for He*(2^3S, 2^1S) + Ca

The electron spectra are calculated according to the following approximate formula [42]:

$$\frac{d\sigma_f}{d\varepsilon}(E_*, E_{+f}) \approx g_* \frac{2\pi^2}{k_*^2} \sum_J (2J+1) e^{-2\,\mathrm{Im}\,\eta_*^J} |\langle F^J_{+f}(E_{+f})| \times \Gamma^{1/2} | F^J_*(E_*)\rangle|^2 \quad (10)$$

where g_* is the statistical weight ($g_* = 1$ for both systems), k_* the asymptotic wave vector and E_* the asymptotic kinetic energy of the entrance channel; $F^J_*(R; E_*)$ and $F^J_{+f}(R; E_{+f})$ are energy normalized radial wavefunctions for the heavy particle motion in the entrance and respective exit channel, η^J_* is the complex phase shift pertaining to F^J_* and E_{+f} is the asymptotic kinetic energy in the exit channel.

The calculated spectra are averaged over the experimental distribution of relative collision energies represented by the following weight factors for the discrete collision energies in the interval 20–160 meV at steps of 10 meV: 0.04, 0.75, 4.42, 12.26, 19.99, 21.95, 17.85, 11.52, 6.23, 2.94, 1.26, 0.50, 0.19, 0.07, 0.02. Such spectra for the $4s$ exit channel are shown in Fig. 6 on a common energy scale. In these spectra the Airy oscillations are clearly resolved and even fast oscillations due to entrance channel ingoing–outgoing wave interference [32, 34] can be seen. In the singlet case these oscillations are damped since the outgoing wave is very weak due to the large ionization rate. The convolution of these spectra with the experimental resolution function (taken to be a gaussian with 60 meV FWHM) removes the detailed structures and reduces the height of the main peak significantly. For comparison with the experimental results the theoretical spectra are combined for each of the exit channels with the experimental triplet-to-singlet flux ratio of 6.9:1 and folded with the experimental resolution function. Since the measured data are known in relative intensity units only, they have been scaled to match the calculated spectra by requiring that the respective He*(2^1S)/($Ca^+(4s)$ contributions have the same area. The corresponding experimental and theoretical spectra are compared in Figs. 7 and 8 for the $4s$ and $4p$ exit channels, respectively. The measured spectra have been corrected for the energy dependent transmission function of the electron spectrometer which was assumed to vary as $\varepsilon^{-1/2}$ (see also Sect. 2). Note that the ordinate scale in Fig. 8 is based on the same normalization as in Fig. 7, but has been magnified with respect to that in Fig. 7 for clarity. The good agreement between the experimental and theoretical peak areas for both 2^3S and 2^1S indicate that the uncertainty in the flux ratio is probably not larger than 10%. The calculated relative intensities for the $2^1S, 2^3S \rightarrow Ca^+(4s)$ and $2^1S, 2^3S \rightarrow Ca^+(4p)$ transitions are 100:64:47:9.6. The corresponding total cross section ratio $2^1S/2^3S$ of 2.00 and the $4p/4s$ branching ratios of 0.47 for 2^1S and 0.15 for 2^3S agree with the experimental values (Table 2) within their uncertainties;

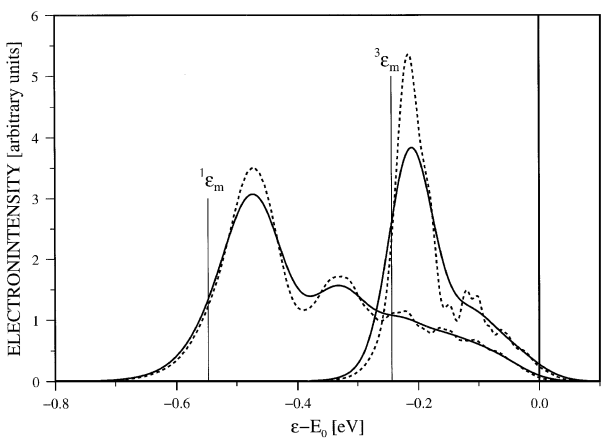

Fig. 6. Theoretical electron energy spectra for the reactions He*(2^1S, 2^3S) + Ca → He + $Ca^+(4s)$ + e^- as calculated for the experimental distribution of collision energies before (*dashed lines*) and after convolution (*full lines*) with the experimental electron energy resolution (60 meV FWHM). The spectral areas correspond to the respective cross sections for $Ca^+(4s)$ formation ($2^3S:2^1S$ ratio 0.64)

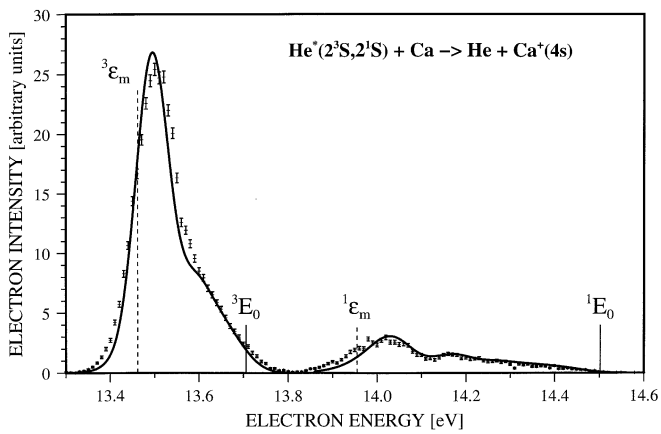

Fig. 7. Comparison of transmission-corrected, background-subtracted experimental electron energy spectra for the reactions He*(2^3S, 2^1S) + Ca → He + $Ca^+(4s)$ + e^- with the calculated spectra (*solid line*). The experimental and theoretical intensity scales were adjusted by matching the areas of the 2^1S spectra. In both Figs. 7 and 8, the experimental He*(2^3S)/He*(2^1S) flux ratio of 6.9 and the relevant collision energy distributions were used in the calculation of the mixed He*(2^3S, 2^1S) spectra; the theoretical nominal energies $^3E_0$ and $^1E_0$ were matched to the experimental values. The *dashed vertical lines*, labelled $^3\varepsilon_m$ and $^1\varepsilon_m$, mark the locations of the respective minima in the classical electron energy functions $\varepsilon(R)$ (2)

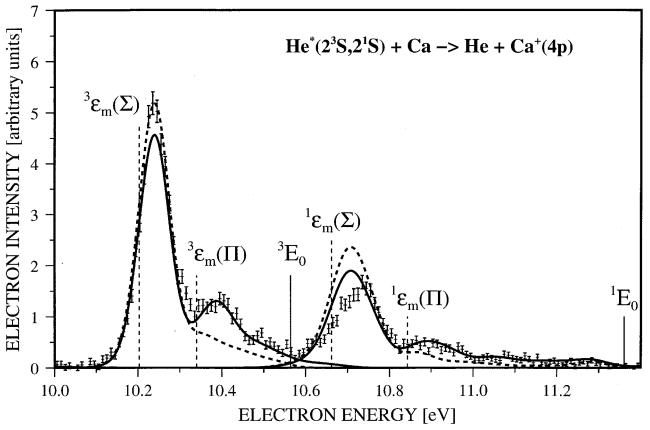

Fig. 8. Comparison of the transmission-corrected, background-subtracted experimental electron energy spectra for the reactions $He^*(2^3S, 2^1S) + Ca \rightarrow He + Ca^+(4p) + e^-$ with the calculated spectra (*dashed line*); in these calculations transitions to the $He + Ca^+(4p)\,^2\Pi$ potentials are practically absent because of the negligible amplitude of the respective autoionization width. The *solid line* represents the results of a modified calculation which includes transitions to the $He + Ca^+(4p)\,^2\Pi$ potential in a semiempirical way (see text). The *dashed vertical lines*, labelled ${}^3\varepsilon_m(\Sigma)$, ${}^3\varepsilon_m(\Pi)$, ${}^1\varepsilon_m(\Sigma)$ or ${}^1\varepsilon_m(\Pi)$, mark the locations of the respective minima in the classical electron energy functions for the outgoing Σ and Π potentials of $He + Ca^+(4p)$. The nominal energies ${}^3E_0$, ${}^1E_0$ have been drawn as obtained from the energy for the $Ca^+(4p)$ multiplet center

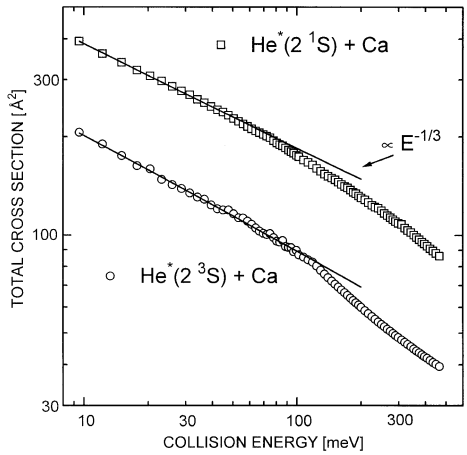

Fig. 9. Energy dependence of the total ionization cross sections in $He^*(2^3S) + Ca$ and $He^*(2^1S) + Ca$ collisions over the range 10–500 meV. At low collision energies the cross sections follow the $E_{rel}^{-1/3}$ dependence (*full lines*) expected from the close collision cross sections for a C_6/R^6 long range attraction (see text)

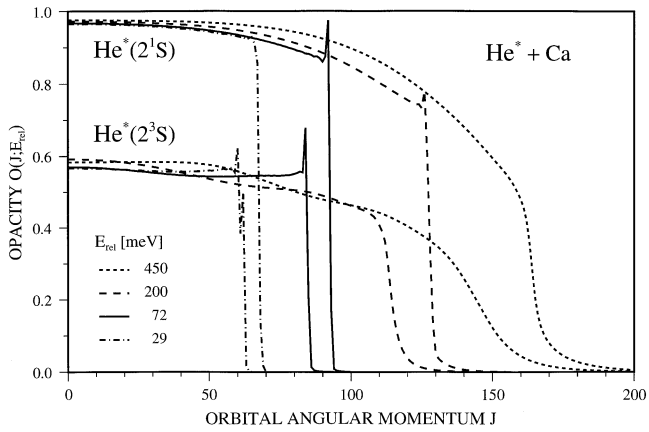

Fig. 10. Dependence of the opacity function $O(J; E_{rel})$ on orbital angular momentum J for ionization in the systems $He^*(2^3S) + Ca$ and $He^*(2^1S) + Ca$ at the four collision energies $E_{rel} = 29$, 72, 200, and 450 meV

the $4p/4s$ ratios are almost independent of collision energy in the range (10–450) meV.

The calculated width functions lead only to the $\Sigma - \Sigma$ transitions (solid line in Fig. 7 and dashed line in Fig. 8). The additional structure in the experimental spectra for the $Ca^+(4p)$ channel (Fig. 8) can be clearly attributed to the Σ–$4p\Pi$ transitions as indicated by the energy positions ${}^3\varepsilon_m(\Pi)$, ${}^1\varepsilon_m(\Pi)$ of the minima in the corresponding difference potentials. As discussed above this is attributed to intensive borrowing due to exit channel coupling not accounted for in the ab initio calculations. Using a branching ratio between the $4p\Sigma$ and $4p\Pi$ channels as suggested by the experimental spectra, we have constructed effective width functions as $\Gamma_{eff}(4p\Sigma) = (1 - c)\Gamma(4p\Sigma)$ and $\Gamma_{eff}(4p\Pi) = c\Gamma(4p\Sigma)$ with $c = 0.12$ and 0.20 for 2^3S and 2^1S, respectively. The solid line in Fig. 8 includes the contribution from the $4p\Pi$ channel obtained in this way. The final electron spectra (solid lines) show good agreement with experiment. Note in particular the full agreement of the low energy edges in the triplet spectra.

The calculated total ionization cross sections are shown in Fig. 9. At the mean collision energy of the present experiment, 72 meV, they amount to 201 Å^2 and 101 Å^2, respectively. The energy dependence of the total ionization cross sections is best understood from the impact parameter dependence of the ionization probabilities, i.e. the dependence of the opacity functions $O(J; E_{rel})$ on orbital angular momentum J. They are shown in Fig. 10 for both $He^*(2^3S) + Ca$ and $He^*(2^1S) + Ca$ at four selected collision energies E_{rel}. The opacities have low-J maxima of about 0.6 for triplet He and 0.96 for singlet He, respectively. At low collision energies ($E_{rel} \ll D_e^*$) the opacities are nearly constant below a critical angular momentum J_c which separates trajectories leading to short distances (close collisions, $J \leq J_c$) from those which do not surmount the rotational barrier located at large distances where the autoionization width is negligible. The ionization cross section is then simply given by the close collision cross section multiplied by the $J < J_c$ average opacity $\bar{O}$, $\sigma_{ion} = \bar{O}\pi b_c^2 = \bar{O}\pi(J_c + 1/2)^2/k_*^2$, where $b = (J + 1/2)/k_*$ is the usual relation between the impact paramter b and the orbital angular momentum quantum number J (k_* = wave vector of relative heavy particle motion). At selected angular momenta near J_c the opacity may increase due to resonance effects; several cases are clearly seen in Fig. 10. Such resonance effects are also responsible for some structure in the ionization cross section [27, 55, 41] as weakly visible in Fig. 9 for $He^*(2^3S) + Ca$. At larger collision energies the opacity functions are smooth and the sharp decrease around J_c is progressively smeared out because the centrifugal

potential shifts the inner turning points away from the region of large Γ, already for J below J_c.

At low energies the cross sections show a dependence on collision energy close to $E_{\mathrm{rel}}^{-1/3}$, as predicted by the "close collision" cross section σ_c for a dispersion type potential with a C_6/R^6 long range attraction. It is given by [53]

$$\sigma_c(E) = (3\pi/2)(2C_6/E_{\mathrm{rel}})^{1/3} \quad \text{(a.u.)}. \tag{11}$$

The opacities of Fig. 10 and the ionization cross sections given in Fig. 9 may be used to derive an effective $\bar{C}_6$ for which $-\bar{C}_6/R^6$ corresponds to the actual potential in the region of the centrifugal barrier for J_c. Due to the higher terms $C_8, C_{10} \ldots$ it should be larger than the calculated C_6 and actually happens to be close to the one obtained from the Slater-Kirkwood formula (5) (Table 3).

To our knowledge only few experimental data for total cross sections of the He* + X systems exist in the literature [8, 22, 54]. Butterfield et al. [54] measured destruction cross sections for He*(2^3S) + X in a low-current low pressure discharge with the pulsed afterglow technique, and obtained 41 Å^2 for X = Ca and 16 Å^2 for X = Sr. The value for Ca is in clear conflict with our calculated value of 101 Å^2 (note that the average collision energy in [54] was probably somewhat smaller than in our experiment and that the destruction cross section represents an upper bound to the total ionization cross section). Total ionization cross sections are available for He* + Mg (2^1S: 38 Å^2, 2^3S: 16 Å^2) from the work of Inaba et al. [8] and for He*(2^3S) + Ba and He*(2^1S) + Ba by Gerard and Hotop [22]. The latter obtained energy dependences over the range 40–400 meV which are quite similar to those calculated here for X = Ca and absolute values of 105 Å^2(2^1S) and 55 Å^2(2^3S), determined at E_{rel} = 100 meV. If we make the assumption that the estimated C_6 of Table 3 give reasonable approximations for close collision cross sections via eq. (11), as is the case for Ca, the measured total cross sections would all imply substantially lower mean opacities than calculated here for Ca. The disagreement in the case of Ca rather seems to indicate substantial difficulties in the accurate measurement of absolute Penning ionization cross sections for metal atoms.

6 Conclusions

In this paper we have reported the first comprehensive electron spectrometric study of Penning ionization occurring in thermal energy collisions (average collision energy $\bar{E}_{\mathrm{rel}}$ around 70 meV) between metastable He*(2^3S) and He*(2^1S) atoms with ground state alkaline earth atoms X (X = Mg, Ca, Sr, Ba). The electron energy resolution (40–70 meV) was sufficiently high to resolve the essential details of the spectra and to deduce reliable estimates for the well-depths D_e^* of the respective entrance channel potentials. Reflecting the stronger long-range forces associated with the higher polarizability of He*(2^1S), the He*(2^1S) + X potentials are found to be about 2.3 times deeper than the respective He*(2^3S) + X potential wells. Besides the dominant formation of the ground ionic exit channel He + $X^+(ms)$, the He + $X^+(mp)$ channel is also populated with substantial probability. The lowest lying He + $X^+[(m-1)d]$ channel is also observed, but attains significant probability only for X = Ba. The spectra for the He + $X^+(mp)$ exit channel reveal that transitions to the respective $^2\Sigma$ potential are mainly involved. This propensity qualitatively explains the formation of polarized $X^+(mp\ ^2P_{3/2})$ ions as observed by Penning ionization optical spectroscopy [19, 20].

In order to provide the basis for deeper understanding of the experimental observations in terms of potentials and local ionization rates and also to provide absolute ionization cross sections we have carried out exemplary ab initio calculations for two of the eight studied systems, namely He*(2^3S) + Ca and He*(2^1S) + Ca, considering the two major exit channels He + $Ca^+(4s, 4p)$. Based on accurate potential curves for the entrance and exit channels and the four autoionization width functions, we have obtained energy dependent total and partial ionization cross sections over the collision energy range (10–450) meV and show angular momentum dependent opacities (i.e. ionization probabilities) at four selected energies. Furthermore we have calculated electron energy spectra for the appropriate experimental conditions and find very good agreement, both in spectral shape and intensities. The He + $Ca^+(4p)$ experimental spectra show small, but clearly resolved contributions due to the $4p\Pi$ channel in spite of the fact that the width function for this continuum turned out negligible. Assuming an R-independent Σ-Π coupling of the width functions, even the small contributions could be well simulated.

So far only few attempts have been made to measure absolute ionization (or destruction) cross sections in collisions between metastable He* atoms and alkaline earth atoms [8, 22, 54]. The value reported for triplet He*(2^3S) + Ca amounts to only 40% of the value calculated here. We would tentatively infer that the other values are also significantly too low.

This work was supported by the Deutsche Forschungsgemeinschaft through Sonderforschungsbereich 91 and grant 436KRO17. AJY and MM gratefully acknowledge the financial support from DFG and the hospitality at Fachbereich Physik and Fachbereich Chemie of the University of Kaiserslautern. We thank G. Koschmann for careful secretarial help with the manuscript.

References

1. Süzer, S., Lee, S.-T., Shirley, D.A.: Phys. Rev. A**13**, 1842 (1976)
2. Hansen, J.E.: Phys. Rev. A**15**, 810 (1977)
3. Cermák, V., Herman, Z.: Chem. Phys. Lett. **2**, 359 (1968)
4. Hotop, H., Niehaus, A.: Z. Phys. **228**, 68 (1969)
5. Cermák, V.: Coll. Czech. Chem. Commun. **36**, 948 (1971)
6. Gerard, K., Hotop, H., Mahr, D.: Adv. Mass. Spectrom. **7A**, 192 (1977)
7. Inaba, S., Goto, T., Hattori, S.: J. Phys. B**14**, 507 (1981); J. Chem. Phys. **75**, 5209 (1981); J. Phys. D**15**, 35 (1982); J. Phys. Soc. Jpn. **51**, 627 (1982)
8. Inaba, S., Goto, T., Hattori, S.: J. Phys. Soc. Jpn. **52**, 1164 (1983)
9. Schearer, L.D.: Phys. Rev. Lett. **22**, 629 (1969)
10. Schearer, L.D., Riseberg, L.A.: Phys. Rev. Lett. **26**, 599 (1971)
11. Parks, W.F., Schearer, L.D.: Phys. Rev. Lett. **29**, 531 (1972)
12. Schearer, L.D.: Phys. Rev. A**10**, 1380 (1974)
13. Green, J.M., Webb, C.E.: J. Phys. B**7**, 1698 (1974)
14. Hamel, J., Margerie, J., Barrat, J.-P.: Opt. Commun. **12**, 409 (1974)
15. Hamel, J., Barrat, J.-P.: Opt. Commun. **18**, 357 (1976)
16. Rambow, F.H.K., Schearer, L.D.: Phys. Rev. A**14**, 1735 (1976)

17. Silfvast, W.T.: Appl. Phys. Lett. **13**, 169 (1968); Phys. Rev. Lett. **27**, 148 (1971)
18. Schearer, L.D., Parks, W.F.: Progr. At. Spectrosc. Part B, pp. 769–775. Hanle, W., Kleinpoppen, H. (eds.) New York: Plenum Press 1979
19. Fahey, D.W., Parks, W.F., Schearer, L.D.: J. Phys. B**12**, L619 (1979)
20. Fahey, D.W., Schearer, L.D., Parks, W.F.: Phys. Rev. A**20**, 1372 (1979)
21. Fuchs, V., Niehaus, A.: Phys. Rev. Lett. **21**, 1136 (1968)
22. Gérard, K., Hotop, H.: Chem. Phys. Lett. **43**, 175 (1976)
23. Arrathoon, R., Littlewood, I.M., Webb, C.E.: Phys. Rev. Lett. **31**, 1168 (1973)
24. Dalidchik, F.I.: Sov. Phys. JETP **41**, 450 (1976)
25. Hotop, H., Ruf, M.-W., Yencha, A.J., Fricke, B.: Ann. Phys. (Lpz.) **47**, 635 (1990)
26. Merz, A., Ruf, M.-W., Hotop, H., Movre, M., Meyer, W.: J. Phys. B**27**, 4973 (1994)
27. Movre, M., Meyer, W., Merz, A., Ruf, M.-W., Hotop, H.: Chem. Phys. Lett. **230**, 276 (1994)
28. Herman, Z., Cermák, V.: Coll. Czech. Chem. Commun. **31**, 649 (1966)
29. Hotop, H., Lorenzen, J., Zastrow, A.: J. Electron. Spectrosc. Rel. Phenom. **23**, 347 (1981)
30. Lorenzen, J., Hotop, H., Ruf, M.-W.: Z. Phys. D**1**, 261 (1986)
31. Ruf, M.-W., Yencha, A.J., Hotop, H.: Z. Phys. D**5**, 9 (1987)
32. Merz, A., Müller, M.W., Ruf, M.-W., Hotop, H., Meyer, W., Movre, M.: Chem. Phys. **145**, 219 (1990)
33. Schohl, S., Müller, M.W., Meijer, H.A.J., Ruf, M.-W., Hotop, H., Morgner, H.: Z. Phys. D**16**, 237 (1990)
34. Müller, M.W., Merz, A., Ruf, M.-W., Hotop, H., Meyer, W., Movre, M.: Z. Phys. D**21**, 89 (1991)
35. Merz, A., Ruf, M.-W., Hotop, H.: Z. Phys. D**32**, 197 (1994)
36. Hotop, H., Kolb, E., Lorenzen, J.: J. Electron. Spectrosc. Rel. Phenom. **16**, 213 (1979)
37. Hotop, H., Niehaus, A.: Z. Phys. **238**, 452 (1970)
38. Miller, W.H.: J. Chem. Phys. **52**, 3563 (1970)
39. Jones, R.O.: J. Chem. Phys. **72**, 3197 (1980)
40. Miller, T.M., Bederson, B.: Adv. At. Mol. Phys. **13**, 1 (1977)
41. Movre, M., Meyer, W.: J. Chem. Phys. (submitted for publication)
42. Hickman, A.P., Morgner, H.: J. Phys. B**9**, 1765 (1976)
43. Müller, W., Flesch, J., Meyer, W.: J. Chem. Phys. **80**, 3297 (1984)
44. Müller, W., Meyer, W.: J. Chem. Phys. **80**, 3311 (1984); Schmidt-Mink, I., Müller, W., Meyer, W.: Chem. Phys. Lett. **112**, 120 (1984); Chem. Phys. **92**, 263 (1985)
45. Walter, C.W., Peterson, J.R.: Phys. Rev. Lett. **68**, 2281 (1992); Peterson, J.R.: Aust. J. Phys. **45**, 293 (1992)
46. Nadeau, M.J., Zhao, X.L., Garwan, M.A., Litherland, A.E.: Phys. Rev. A**46**, R3588 (1992)
47. van der Hart, H.W., Laughlin, C., Hansen, J.E.: Phys. Rev. Lett. **71**, 1506 (1993)
48. Feshbach, H.: Ann. Phys. (N.Y.) **5**, 357 (1958); ibid. **19**, 287 (1962)
49. Langhoff, P.W.: Int. J. Quant. Chem. Symp. **8**, 347 (1974)
50. Hazi, A.U.: J. Phys. B**11**, L259 (1978)
51. Meyer, W.: J. Chem. Phys. **64**, 290 (1976); Werner, H.-J., Reinsch, E.-A.: J. Chem. Phys. **76**, 3144 (1982)
52. Moore, C.E.: Atomic Energy Levels, NSRDS-NBS **35** (1971)
53. Bell, K.L., Dalgarno, A., Kingston, A.E.: J. Phys. B**1**, 18 (1968)
54. Butterfield, K.B., Gerstenberger, D.C., Shay, T., Little, W.L., Collins, G.J.: J. Appl. Phys. **49**, 3088 (1978)
55. Brutschy, B., Haberland, H., Schmidt, K.: J. Phys. B**9**, 2693 (1976)